MATERIALS PHYSICS AND MECHANICS RESEARCH ARTICLE

Submitted: September 13, 2024 Revised: August 26, 2025 Accepted: September 10, 2025

Double diffusive convection of non-Newtonian nanofluid in porous layer under internal heating

V. Sharma [1], J. Devi [2]✉, R. Kumar [3], V. Sharma [2]

[1] Govt. College, Tissa, Chamba, Himachal Pradesh, India

[2] Himachal Pradesh University, Shimla, India

[3] Kurukshetra University, Kurukshetra, Haryana, India

✉thakurjyoti641@gmail.com

ABSTRACT

The onset of double-diffusive convection in a non-Newtonian nanofluid-saturated porous layer is investigated under the effect of internal heating and various boundary conditions. A non-Newtonian nanofluid is modeled using the Buongiorno framework for nanoparticles combined with the Jeffrey model for viscoelastic fluid behavior. The governing coupled differential equations are reduced to ordinary linear differential equations via the normal mode method, the Boussinesq approximation, and linear stability analysis. Eigenvalue problems are solved using realistic boundary conditions to determine the stationary Rayleigh numbers, which describe the initiation of non-oscillatory convection in terms of non-dimensional controlling parameters. This work is motivated by practical applications in geophysics, energy engineering, and materials science, where non-Newtonian nanofluids in porous layers are subjected to internal heating, such as in geothermal reservoirs, enhanced oil recovery, and thermal management systems. The analysis demonstrates that reduced particle density and internal heating promote convection, whereas porosity, solutal Rayleigh number, concentration Rayleigh number, and modified diffusivity ratio stabilize the system. Furthermore, reduced particle density enhances instability, while the Jeffrey parameter introduces viscoelastic effects that weaken stability without altering convection cell size. These findings provide new insights into the stabilization and destabilization mechanisms of nanofluid systems, with implications for designing advanced energy and material processing technologies.

KEYWORDS

Internal heat source • Jeffrey model • double diffusive convection • porous material

Citation: Sharma V, Devi J, Kumar R, Sharma V. Double diffusive convection of non-Newtonian nanofluid in porous layer under internal heating. *Materials Physics and Mechanics*.2025;53(4): 76–90.
http://dx.doi.org/10.18149/MPM.5342025_6

Introduction

A type of convection called double diffusive convection is driven by two slopes that have different diffusion rates. Several industrial areas are very interested in this phenomenon, such as putting nuclear waste underground, making binary mixtures solid, electrochemistry, magma chambers, the earth's oceans, and oil drilling. This convection also helps us understand how convection works in the sun, where warmth and helium move around at different speeds. A lot of study has been done on the phenomenon of double diffusive convection, especially in relation to salt fingers in oceanic settings. Stern [1] wrote about the conditions that allow rhythmic motion to be seen, meaning that warmer, saltier water is below colder, less dense water. Huppert and Turner [2], on the other hand, found that binary convection (double diffusive convection) can happen with two parts in the fluid layer and cause motion to stop in the shape of salt-fingers. Dougall [3] did a thorough study on binary convection in a solute-solute pair caused by molecular diffusion. Kafoussias and Williams [4] did a study to look at how the Soret and Dufour factors affected boundary layer flow in laminar mixed convection and mass transport with viscosity that changes with temperature. Kuznetsov and Sheremet [5] also did a numerical study on binary convection in holes with Soret and Dufour effects, taking into account heat transfer through solid walls. Lotfy et al. [6] analyzed Hall current and microtemperature effects on rods, and ramp-type microtemperature heating in rotator semiconductors, highlighting coupled elastic, magnetic, plasma, and thermal interactions. Lotfy et al. [7] applied hyperbolic two-temperature theory in 1D, showing strong effects on displacement, stress, and carrier density. Lotfy and El-Bary [8] extended this to 2D microstretch models under photothermal transport, while Ismail et al. [9] examined variable thermal conductivity impacts on thermal-plasma-elastic waves. These studies underscore the critical role of coupled mechanical, thermal, and electromagnetic effects in optimizing semiconductor behavior.

Researchers are very interested in using nanofluids because they have unique properties that make them better at conducting heat. These properties come from mixing nanoscale particles (such as oxide ceramics, metal carbides, nitrides, and metals or carbon nanotubes) with a base fluid (such as ethylene or triethylene glycols, water, alcohol, and polymer solutions), with Choi [10] being the first person to suggest this idea. These fluids are used for many different things, such as making nano-composites, bio-pharmaceuticals, oil digging, building nanostructures for transportation, and cooling electronics. Nanoparticles come in different types, each with its own unique optical, magnetic, mechanical, and thermal qualities. These include metal oxide ceramics like Al_2O_3 or CuO, ZnO, and TiO_2, nitrides ceramics like AlN or SiN, and metals. A lot of experts have made a lot of models to show how well nanofluids conduct heat. Maxwell [11] was the first person to study the thermal conductivity of colloidal solutions. This is a comparison of the thermal conductivity of fluids and particles. The Lattice Boltzmann model was used by Xuan et al. [12] to look into how heat moves through nanofluids. Buongiorno [13] studied nanofluid transport to find out how the relative speeds of nanoparticles in a normal fluid and a fluid with nanoparticles could be compared. A lot of researchers have used the modified conservation equations of motion to look into how thermal instability starts in nanofluids and nanoparticles, taking into account the effects of Brownian diffusion and thermophoresis. The main goal of the studies was to look into various mixtures of parameters and boundary conditions, either by themselves or with others.

Unlike the Oldroyd-B or Maxwell models, the Jeffrey model employs a single relaxation parameter that efficiently captures the viscoelastic behavior of the fluid without overcomplicating the governing equations. Jeffrey Nanofluid is a type of nanofluid that contains tiny particles mixed into a Jeffrey fluid. A Jeffrey fluid is a non-Newtonian fluid that shows shear thinning behavior, which means that as shear rate increases, viscosity decreases. Adding nanoparticles can improve the fluid's thermal and rheological qualities, which means it can be used in more situations. Some of these uses are making polymers, coatings, and composites better and more durable, controlling spacecraft, satellites, and other aerospace systems, and improving the performance and thermal efficiency of solar collectors and other energy systems. Additionally, Jeffrey

Nanofluid can be used in heat sinks, drug delivery, tissue engineering, and other biological tasks. It can also be used as a drilling fluid or a hydraulic fracturing fluid.

A lot of people are interested in studying double diffusive convection in Jeffrey nanofluid flooded porous layers because it has many uses in energy systems, environmental engineering, and industrial processes. A lot of research has been done to look into what happens when two types of convection mix in a layer that is both fluid and porous and full of nanoparticles. Umavathi and Sasso [14] looked into convection in a binary porous layer that was filled with an Oldroyd nanofluid. Yadav et al. [15] looked into the phenomenon of binary convective motion in a porous layer filled with Kuvshiniski fluid. They found that raising the Kuvshiniski parameter lowers convective heat transfer while raising the thermal Rayleigh number and the solute Rayleigh number increases both heat and mass transfers. Shoaib et al. [16] looked into the two-way flow of nanofluid on a flat, sloped surface that was saturated and porous. To do a full analysis, their study used an AI-based system with a balanced back propagated network. According to the results, as Gr goes up, so does velocity. The magnetic field parameter and angle of inclination, on the other hand, show the reverse trend.

More and more people are interested in studying free convection in fluids that contain internal energy. This is mostly because nuclear power engineering needs to get better all the time. The study of convection caused by internal heat sources has many uses in many fields, such as astrophysics, geophysics, thermal ignition, downsizing electrical parts, fire dynamics, combustion processes, and more. Researchers are looking into how an internal heat source affects the start of thermal convection in different types of fluids because the heat source makes the fluids float more, which changes the way heat and mass move through them. Experiments and computer simulations have both been used to look into how internal warmth affects natural convection in classical fluids. Sparrow et al. [17] looked at how internal warmth affects free convection and found that it makes the fluid layer more likely to become unstable. Watson [18] looked at how both internal heat sources and sinks affected the system and found that both of them made it less stable. Israel-Cookey et al. [19] looked into how thermally unstable a porous fluid layer is when internal warmth is added. The Darcy-Brinkman model was used by Yadav et al. [20] to look at how an internal temperature affects the start of nanofluid convection in a porous medium. The researchers found that the porosity has a calming effect on the system and the nanofluid Lewis number has an unstable effect. Sharma and Sharma [21] examined influence of heat sources and relaxation time on temperature distribution in tissues. Altawallbeh [22] did research on binary convection in a viscoelastic fluid porous layer with an internal heating. They found that when the thermal Rayleigh number is below the critical value, an increase in internal heat causes the Sherwood number to drop. Combined effects of Brownian motion and viscous dissipation on heat transfer and temperature distribution of Al_2O_3 /water nanofluid flow through a porous medium have been explored by Bouazizi and Turki [23]. Sharma and Khator [24,25] explored some problems of renewable sources with regard to power generation planning. A study by Ali et al. [26] used numbers to look into convection in a binary anisotropic porous layer that was rotated and heated from the inside. They found that warmth from the inside speeds up heat transfer, which makes it easier for thermal convection to start inside the system. The nanofluids' viscosity prediction through interaction layer of particle-media have been investigated by Syzrantsev et al. [27] and draw fundamental understanding of the rheology of nanofluids (dispersions based on SiO_2 and Al_2O_3 nanoparticles). Abo-Dahab et al. [28] studied numerical estimation of the Double diffusive peristaltic flow of non- Newtonian Sisko nanofluid through a porous medium inside a horizontal symmetrical flexible channel under the various impacts due to specific boundary restrictions. Paandurangan et al. [29] investigated the heat and mass transfer in mixed convection peristaltic flow of Casson nanofluid through an asymmetric permeable channel filled with a porous medium in the presence of electro osmosis.

Recent advancements in porous media modeling have highlighted the importance of fractional and nonlocal approaches to capture anomalous diffusion and long-range interactions [30−32]. Such models allow accurate representation of spatio-temporal heat transfer and microstructural effects in complex media. Simultaneously, thermoelastic and viscoelastic nanofluids have gained prominence in energy systems, including solar collectors and thermal management devices, where enhanced heat transfer and stability are crucial [33,34]. Incorporating viscoelastic fluid behavior with advanced nanofluid formulations enables better prediction and control of convective processes, bridging the gap between theoretical modeling and practical energy applications. Raza et al. [35] investigated that nanofluids offer superior thermal conductivity compared to conventional fluids, with hybrid types like Al_2O_3−MWCNT enhancing heat transfer by up to 79 %. Their complex behavior challenges standard numerical methods, making multiscale modeling and AI-based techniques such as ANN, CNN, and RNN essential for predicting thermophysical stability and optimizing performance. Integrating experimental results with computational and AI-driven models is key for developing efficient, scalable nanofluid-based thermal systems.

Although the present study uses classical integer-order derivatives, the framework can be extended to include fractional-order or non-local effects, enabling the modeling of memory-dependent transport and long-range interactions in porous media. Such extensions would allow a more accurate representation of anomalous diffusion and complex thermal responses in nanofluid systems.

Because internal heat sources can be used in many different ways, we looked into how internal heat sources affect the start of binary convection in nanofluids with changed boundary conditions. Using the Jeffrey model with no nanoparticle volumetric flow helps to explain the rheology of the fluids. Unlike earlier works that studied Newtonian nanofluids or simplified viscosity models, our approach captures the influence of viscoelastic effects (through the Jeffrey parameter) together with nanoparticle migration and internal heating. This provides a more realistic framework for non-Newtonian nanofluid convection extending traditional models and offering improved predictive capability for thermoelastic behavior in porous structures.

Mathematical formulation

Two parallel xy lines hold in place a horizontal layer of a binary Jeffrey nanofluid that can't be squished. The temperatures in the lower and upper planes are shown as T_0 and T_1 at $z = 0$ and $z = d$ respectively with $(T_0 > T_1)$. The system is given a small temperature difference, $\left|\frac{dT}{dz}\right|$ and the nanofluid has a constant heat source inside it, Q_0. The system is also affected by a gravity field, $g(0,0,-g)$ which can be seen in Fig. 1.

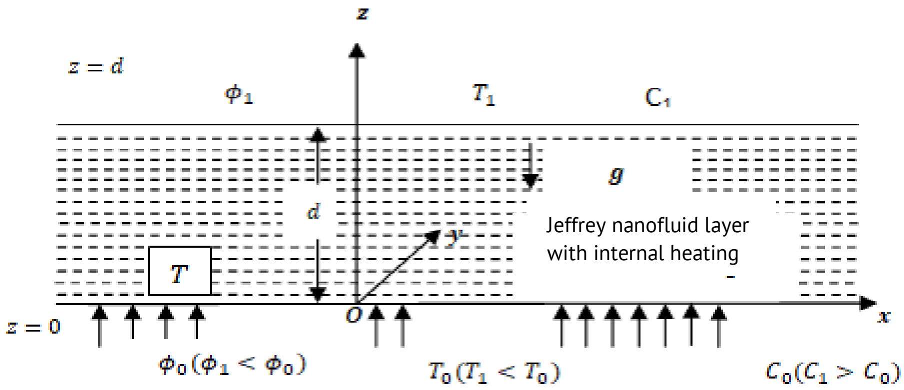

Fig. 1. Geometrical configuration of the system

The model is built under the following assumptions:
1. The nanofluid is incompressible and satisfies the Boussinesq approximation.
2. The porous medium obeys Darcy's law.
3. Fluid rheology follows the Jeffrey viscoelastic model.
4. Nanoparticle transport is governed by the Buongiorno model, including Brownian diffusion and thermophoresis.
5. Heat generation within the porous layer is uniform.
6. All thermophysical properties are constant except density in the buoyancy term.
7. Boundary conditions are taken as realistic experimental configurations. These assumptions simplify the coupled governing equations into an eigenvalue problem, solved by the Galerkin approach.

The equations that describe the flow, concentration, momentum, and thermal energy of Jeffrey nanofluid under the Boussinesq approach are [13,20,36–40]:

$$\nabla \cdot q = 0, \tag{1}$$

$$\frac{\rho}{\varepsilon}\left[\frac{\partial q}{\partial t} + \frac{1}{\varepsilon}(q \cdot \nabla)q\right] = \left[\phi\rho_p + (1-\phi)\rho_f\{1 - \beta(T - T_0) + \beta'(C - C_0)\}\right]g - \nabla p - \frac{\mu}{(1+\lambda)}\frac{q}{k_1}, \tag{2}$$

$$\frac{\partial \phi}{\partial t} + \frac{1}{\varepsilon}(q \cdot \nabla)\phi = \nabla.\left[D_B\nabla\phi + \frac{D_T}{T_0}\nabla T\right], \tag{3}$$

$$(\rho c)_m\frac{\partial T}{\partial t} + \frac{(\rho c)_f}{\varepsilon}(q \cdot \nabla)T = \nabla.(k_T.\nabla T) + (\rho c)_p\nabla T.\left[D_B\nabla\phi_n + \frac{D_T}{T_0}\nabla T\right] + Q_0, \tag{4}$$

$$(\rho c)_m\frac{\partial C}{\partial t} + \frac{(\rho c)_f}{\varepsilon}(q \cdot \nabla)C = \nabla.(k_c.\nabla C). \tag{5}$$

Different symbols in the above equations stand for different amounts of matter. Here, $\boldsymbol{q}$, $\boldsymbol{g}$, T, C, p, $\varepsilon, \lambda, \rho_p$, ρ_f, ϕ, β, β', k_1 and μ stand for the Darcy speed, the acceleration due to gravity, the temperature, the concentration, the pressure, the porosity, the Jeffrey parameter, the density of the nanoparticles, the density of the base fluid, the volume fraction of the nanoparticles, the thermal expansion coefficient, the solute expansion coefficient, the permeability of the porous medium, and the viscosity. Also, $(\rho c)_f$,$(\rho c)_p$,$(\rho c)_m$, D_B, K_T, k_c and D_T stand for the heat capacity of the fluid, the heat capacity of nanoparticles, the heat capacity of the fluid in a porous medium, the Brownian diffusion coefficient, the thermal conductivity, the solute diffusivity, and the thermophoretic diffusion coefficient. Dufour type and Soret type diffusion are not taken into account. Adding a term called "Q_0" to the heat equation is a typical way to deal with an internal heat source.

It is thought that both limits are stress-free and keep their temperatures the same. There is also a small amount of volume fraction flow of nanoparticles. As a result, the following border conditions must be met:

$$\begin{aligned} &w = 0,\ T = T_0,\ C = C_0,\ D_B \frac{\partial \phi}{\partial z} + \frac{D_T}{T_1}\frac{\partial T}{\partial z} = 0 \text{ at } z = 0, \\ &w = 0,\ T = T_1,\ C = C_1,\ D_B \frac{\partial \phi}{\partial z} + \frac{D_T}{T_1}\frac{\partial T}{\partial z} = 0 \text{ at } z = d. \end{aligned} \tag{6}$$

This reflects the physical reality that nanoparticles cannot penetrate solid boundaries, making the setup experimentally realizable. The base concentration and solute profiles are assumed linear, representing an initially uniform preparation of the nanofluid. These boundary conditions allow accurate modeling of the coupled transport of heat, solute, and nanoparticles, capturing the essential physics of double-diffusive convection in a confined porous medium while maintaining consistency with laboratory conditions.

Introducing the variables with no dimensions such as:

$$\begin{aligned} &(x^*, y^*, z^*) = \frac{(x,y,z)}{d}, q^* = \frac{d}{\alpha_m} q, \quad t^* = \frac{\alpha_m}{\sigma d^2} t, \quad \phi_n^* = \frac{(\phi_n - \phi_0)}{(\phi_1 - \phi_0)}, \\ &{q_d}^* = \frac{d}{\alpha_m} q_d, C^* = \frac{(C - C_0)}{\Delta C}, T^* = \frac{(T - T_0)}{\Delta T}, p^* = \frac{p k_1}{\mu \alpha_m}, \end{aligned} \tag{7}$$

we can write Eq. (1) through Eq. (5) in a form that doesn't involve dimensions by changing α_m to $\frac{k_T}{(\rho c)_f}$, σ to $\frac{(\rho c)_m}{(\rho c)_f}$ and ΔT to $T_0 - T_1$:

$$\nabla \cdot q = 0, \tag{8}$$

$$\frac{1}{V_a}\left\{\frac{1}{\sigma}\frac{\partial}{\partial t} + \frac{1}{\varepsilon} q.\nabla\right\} q \frac{D_a}{\varepsilon P_r} = -\frac{q}{1+\lambda} - \nabla p - R_n \phi - R_m + R_a T - \frac{R_s C}{L_e}, \tag{9}$$

$$\frac{\partial T}{\partial t} + \frac{1}{\varepsilon}(q \cdot \nabla) T = \nabla^2 T + \frac{N_B}{L_n}(\nabla \phi_n . \nabla T) + \frac{N_A N_B}{L_e}(\nabla T . \nabla T) + H_s, \tag{10}$$

$$\frac{1}{\sigma}\frac{\partial \phi}{\partial t} + \frac{1}{\varepsilon}(q \cdot \nabla)\phi = \frac{1}{L_n}\nabla^2 \phi + \frac{N_A}{L_n}\nabla^2 T, \tag{11}$$

$$\frac{\partial C}{\partial t} + \frac{1}{\varepsilon}(q \cdot \nabla) C = \frac{1}{L_e}\nabla^2 C. \tag{12}$$

Here $R_m = \frac{[\phi_0 \rho_P + (1-\phi_0)\rho\,] g d k_1}{\mu \alpha_m}$ is the basic density Rayleigh number, $R_s = \frac{\rho\, g \beta d k_1 (\,C_0 - C_1)}{\mu^* \alpha_m}$ is the thermal Rayleigh number $N_A = \frac{D_T\,(\,T_0 - T_1)}{D_B\, T_0\,(\phi_1 - \phi_0)}$ is the modified diffusivity ratio, $N_B = \frac{\varepsilon (\rho c)_P (\phi_1 - \phi_0)}{(\rho c)_f}$ is the modified particle density increment. We have $D_a = \frac{k_1}{d^2}$, the Darcy number, $P_r = \frac{\mu}{\rho\, \alpha_m}$, the Prandtl number, $V_a = \frac{\varepsilon Pr}{Da}$, the Vadasz number, $L_n = \frac{\alpha_m}{D_B}$, the Lewis number, $L_e = \frac{\alpha_m}{k_c}$, the Lewis number due to salinity, $R_a = \frac{\rho\, g \beta d k_1 (\,T_0 - T_1)}{\mu^* \alpha_m}$, the thermal Rayleigh number and $R_n = \frac{(\rho_P - \rho_f\,)(\phi_1 - \phi_0) g d k_1}{\mu \alpha_m}$, the concentration Rayleigh number. The dimensionless internal heat parameter is shown by The dimensionless internal heat parameter is shown by $H_s = \frac{Q_0 d^2}{k_T\,(\,T_1 - T_0)}$.

Basic flow and perturbation equations

We look at a nanofluid that doesn't move or settle over time and doesn't have any floating nanoparticles. It is thought that changes in temperature, pressure, and the bulk fraction of nanoparticles only happen in the z-direction. In this case, the answers to Eq. (8) through Eq. (12) lead to this state:

$$q_b = (0,0,0), p = p_b(z), T = T_b(z), \phi = \phi_b(z), C = C_b(z). \tag{13}$$

Using Eq. (13), Eqs. (8)−(12) give:

$$\frac{\partial^2 T_b}{\partial z^2} + \frac{\partial T_b}{\partial z}\left(\frac{N_B}{L_n}\frac{d\phi_b}{dz} + \frac{N_A N_B}{L_e}\frac{\partial T}{\partial z}\right) + H_s = 0, \tag{14}$$

$$N_A \frac{\partial^2 T_b}{\partial z^2} + \frac{\partial^2 \phi_b}{\partial z^2} = 0, \tag{15}$$

$$\frac{1}{L_e}\frac{\partial^2 C_b}{\partial z^2} = 0. \tag{16}$$

When you do a single integration of Eq. (15) with respect to variable z and include the boundary surfaces (6), you get:

$$N_A \frac{\partial T_b}{\partial z} + \frac{\partial \phi_b}{\partial z} = 0. \tag{17}$$

When you plug in Eq. (17) into Eq. (14), you get:

$$\frac{\partial^2 T_b}{\partial z^2} + H_s = 0. \tag{18}$$

When we do a double integration of Eq. (18) with respect to the variable z and keep the border conditions (6) in mind, we get the following result:

$$T_b = \left(\frac{H_s}{2} - 1\right) z - \frac{H_s}{2} z^2 + 1. \tag{19}$$

Putting Eq. (19) into Eq. (17) and integrating gives us:

$$\phi_b = -\frac{N_A}{2}(-2 - 2H_s z + H_s), \tag{20}$$

$$C_b = -z + 1. \tag{21}$$

To check the stability of the physical system under study, tiny changes are made to the starting flow. This lets us look more closely at:

$$q = q_b + q', T = T_b + T', \phi = \phi_b + \phi', C = C_b + C', \tag{22}$$

where $q' = (u', v', w')$, T', $C'$and ϕ' are the changes in physical quantities.

By using Eqs. (19)−(21), along with perturbations from Eq. (22) in Eq. (8)−(12), we get the non-dimensional linear perturbed equations that look like this:

$$\left\{\frac{1}{\sigma V_a}\frac{\partial q}{\partial t}\right\} = -\frac{q}{1+\lambda} - \nabla p - R_n \phi + R_a T - \frac{R_s C}{L_e}, \tag{23}$$

$$\frac{\partial T}{\partial t} + \frac{q}{2\varepsilon}(H_s - 2 - 2H_s z) = \nabla^2 T + \frac{N_B}{2L_n}(H_s - 2 - 2H_s z)\frac{\partial \phi}{\partial z} + \frac{N_A N_B}{2L_n}(H_s - 2 - 2H_s z)\frac{\partial T}{\partial z}, \tag{24}$$

$$\frac{1}{\sigma}\frac{\partial \phi}{\partial t} + \frac{q}{2\varepsilon}(1 - H_s + 2H_s z)N_A = \frac{1}{L_n}\nabla^2 \phi + \frac{N_A}{L_n}\nabla^2 T, \tag{25}$$

$$\frac{\partial C}{\partial t} - \frac{q}{\varepsilon} = \frac{1}{L_e}\nabla^2 C. \tag{26}$$

We get the following expression when we take variable p out of Eq. (23):

$$\left\{\frac{1}{\sigma V_a}\frac{\partial}{\partial t} + \frac{1}{1+\lambda}\right\}\nabla^2 w = \left(-R_n \nabla_1^2 \phi + R_a \nabla_1^2 T - \frac{R_s \nabla_1^2 C}{L_e}\right). \tag{27}$$

To get exact answers for Eqs. (23)−(26), we use a normal mode analysis to look into the changed physical values. In this method, the variables are given horizontal wave numbers and a growth rate as:

$$[[w', T', C', \phi'] = [W, \Theta, \Psi, \Phi](z)\, exp\{st + i(k_x x + k_y y)\}, \tag{28}$$

where k_x, $k_y$and s all mean what they're supposed to.

Using Eq. (28) along with Eqs. (23)–(27) and making sure that conditions (19), (20), and (21) are met, we can get the following set of stability equations:

$$\left(\frac{1}{\sigma V_a}s+\frac{1}{1+\lambda}\right)(D^2-a^2)W=\left[\left\{R_n a^2\phi+R_a a^2 T-\frac{R_s a^2 C}{L_e}\right\}\right], \tag{29}$$

$$s\Theta+\frac{W}{2\varepsilon}(H_s-2-2H_s z)=\left[(D^2-a^2)\Theta+\frac{N_B}{2L_n}(H_s-2-2H_s z)D\Phi+\frac{N_A N_B}{2L_n}(H_s-\right.$$
$$\left.-2-2H_s z)D\Theta\right], \tag{30}$$

$$s\Psi-\frac{W}{\varepsilon}=\frac{1}{L_e}(D^2-a^2)\Psi, \tag{31}$$

$$\frac{1}{\sigma}s\Phi+\frac{W}{2\varepsilon}(1+2H_s z-H_s)N_A=\frac{1}{L_n}(D^2-a^2)\Phi+\frac{N_A}{L_n}(D^2-a^2)\Theta. \tag{32}$$

The boundary conditions (6) change to:

$$W=D^2W=0,\ D\Phi+N_A D\Theta=0,\ \Theta=0,\ \Psi=0,\ D\Psi=0,\text{ at } z=0 \text{ and } z=1. \tag{33}$$

There is a linear eigenvalue problem for the temperature Rayleigh number that is made up of Eqs. (29)–(32) and boundary conditions (33). We use the Galerkin method to find exact solutions to Eqs. (29)–(32) that don't are easy and meet the boundary conditions (33). For example:

$$W=A_1\sin\pi z,\ \Theta=B_1\sin\pi z,\ \Phi=-C_1 N_A\sin\pi z,\ \Psi=D_1\sin\pi z, \tag{34}$$

where A_1, B_1, C_1 and $D_1$are unknown coefficients.

We can find the thermal Rayleigh number for stationary convection by putting s = 0 in Eqs. (29)–(32) and integrating each equation separately over the range of $0 < z < 1$ while applying the boundary conditions (33). There, we have it:

$$R_a^s=\frac{(\pi^2+a^2)\{a^2+\pi^2\}\varepsilon\{(\pi^2+a^2)L_n+H_s N_A N_B(1+N_A)\}}{a^2(1+\lambda)\{(\pi^2+a^2)+H_s N_A^2 N_B\}}+\frac{N_A^2\{-(\pi^2+a^2)\{1-L_n\}+H_s N_A N_B\}R_n}{\{(\pi^2+a^2)+H_s N_A^2 N_B\}}+$$
$$+\frac{(\pi^2+a^2)\{(\pi^2+a^2)L_n+H_s N_A N_B(1+N_A)\}R_s}{a^2 L_n\{(\pi^2+a^2)+H_s N_A^2 N_B\}}. \tag{35}$$

Now special cases arise:

Case (I): for case (I), if the fluid base is very thick and doesn't have any heat sources inside it ($\lambda=0, H_s=0,$) Eq. (35) reduces to:

$$R_a^s=\frac{(\pi^2+a^2)^2}{a^2}-\frac{(L_e+\varepsilon)N_A R_n}{\varepsilon}+\frac{R_s}{\varepsilon}, \tag{36}$$

the results found are very similar to those of the previous study by Yadav et al. [20].

Case (II): If there are no nanoparticles or salt, i.e.,$R_s=0, R_n=0, N_A=0$, Eq. (36) gets even smaller, to:

$$R_a^s=\frac{(\pi^2+a^2)^2}{a^2}, \tag{37}$$

the result that was seen is in line with what Lapwood [41] found.

We use a mathematical expression $\left(\frac{dR_a^s}{da^2}\right)_{a^2=a_c^2}=0$ to find the critical wave number and its corresponding critical stationary thermal Rayleigh number R_a^s. This gives us a polynomial equation with the variable a_c^2as:

$$\varepsilon L_n^2(a_c^2)^4+2L_n^2(a_c^2)^3\varepsilon(\pi^2+H_s N_A^2 N_B)+(a_c^2)^2 H_s L_n N_A^2 N_B[\{\varepsilon H_s N_A(1+N_A)N_B+$$
$$+L_n(\pi^2(3)\varepsilon+(1+\lambda)N_A^2 R_n)\}-(1+\lambda)\{\pi^2 L_n+H_s N_A(1+N_A)N_B\}R_s-$$
$$-H_s N_A N_B L_n\{(1+N_A)(\pi^2\varepsilon)+(1+\lambda)N_A^2 R_n-(1+\lambda)N_A R_S\}]-2a_c^2\pi^2\{L_n\pi^2+$$
$$+H_s N_A N_B(1+N_A)\}\{\pi^2\varepsilon L_n+(1+\lambda)\}-\pi^2\{\pi^2+H_s N_A^2 N_B\}\{(L_n\pi^2+$$
$$+H_s N_A N_B(1+N_A))(\pi^2\varepsilon L_n+(1+\lambda)R_s)\}=0. \tag{38}$$

If the fluid is regular and there is no salt in it or any internal heating, i.e., $N_A = R_n = 0$, $R_s = 0$ and $H_s = 0$, then Eq. (38) gives us the critical wave number ($a_c = \pi$) and the critical thermal Rayleigh number ($Ra_c = 4\pi^2$), which is very close to what Lapwood [41] suggested.

The effect of the dimensionless parameters H_s, λ, R_s, R_n and L_n on the stationary convection for Jeffrey nanofluid is studied by figuring out $\frac{\partial R_a^s}{\partial H_s}, \frac{\partial R_a^s}{\partial \lambda}, \frac{\partial R_a^s}{\partial R_s}, \frac{\partial R_a^s}{\partial R_n}$ and $\frac{\partial R_a^s}{\partial L_n}$. If you plug in Eq. (35), you get:

$$\frac{\partial R_a^s}{\partial H_s} = \frac{(a^2+\pi^2)[\{1+(1-L_n)N_A\}]N_A N_B[(a^2+\pi^2)\varepsilon + a^2(1+\lambda)N^2{}_A R_n]}{a^2(1+\lambda)\{(a^2+\pi^2)+H_s N_A^2 N_B\}^2}. \tag{39}$$

From Eq. (39) we can see that $\frac{\partial R_a^s}{\partial H_s} > 0$ or < 0 for $1 > L_n$ or $1 < L_n$. But $1 > L_n$ is not possible with the parameter numbers that were chosen. Because of this, an internal heat source makes a machine less stable.

Equation (35), which gives:

$$\frac{\partial R_a^s}{\partial \lambda} = \frac{(a^2+\pi^2)[(a^2)]\varepsilon[(a^2+\pi^2)L_n + H_s N_A N_B(1+N_A)]}{a^2(1+\lambda)^2\{(a^2+\pi^2)+H_s N_A^2 N_B\}}, \tag{40}$$

where Eq. (40) demonstrates that $\frac{\partial R_a^s}{\partial \lambda} > 0$. As a result, the Jeffrey constant makes the system under consideration more stable:

$$\frac{\partial R_a^s}{\partial R_s} = \frac{(a^2+\pi^2)(1+b)[(a^2+\pi^2)L_n + H_s N_A N_B(1+N_A)]}{a^2 L_n\{(1+b)(a^2+\pi^2)+H_s N_A^2 N_B\}}, \tag{41}$$

where Eq. (41) shows that $\frac{\partial R_a^s}{\partial R_s}$ is positive for all wave numbers. Thus, the Rayleigh number due to salinity enhances the stability of system.

$$\frac{\partial R_a^s}{\partial R_n} = \frac{N_A^2[(a^2+\pi^2)(L_n-1)+H_s N_B N_A]}{\{(a^2+\pi^2)+H_s N_B N_A^2\}}. \tag{42}$$

That means $\frac{\partial R_a^s}{\partial R_n}$is positive for L_n greater than 1. In this way, the concentration Rayleigh number makes a system more stable:

$$\frac{\partial R_a^s}{\partial L_n} = \frac{L_n\{(a^2+\pi^2)^2\{a^2+\pi^2\}\varepsilon + a^2(1+\lambda)(a^2+\pi^2)N_A^2 R_n\}}{a^2(1+\lambda)L_n\{(a^2+\pi^2)+N_B H_s N_A^2\}} + \frac{(a^2+\pi^2)^2(1+\lambda)R_s}{a^2(1+\lambda)L_n\{(a^2+\pi^2)+N_B H_s N_A^2\}} - \\ - \frac{(a^2+\pi^2)[(a^2+\pi^2)L_n + H_s N_A N_B(1+N_A)]R_s}{a^2 L^2{}_n\{(a^2+\pi^2)+N_B H_s N_A^2\}}, \tag{43}$$

where Eq. (43) shows that $\frac{\partial R_a^s}{\partial L_n}$is positive for all wave numbers, which implies that L_n has stabilizing influence.

The novelty of this study lies in combining the Jeffrey viscoelastic fluid model with the Buongiorno nanofluid framework to investigate double-diffusive convection under internal heat generation. Internal heating supplies energy directly within the porous nanofluid layer, creating additional buoyancy forces that drive fluid motion even in the absence of external temperature gradients. This reduces the critical thermal Rayleigh number, causing convection to onset earlier and convective cells to grow larger. The Jeffrey viscoelastic fluid, with its elastic (memory) and viscous (damping) characteristics, interacts with buoyancy forces in a manner that amplifies disturbances rather than suppressing them. Interestingly, while previous studies often report that the Jeffrey parameter stabilizes the system and internal heating alone acts as a destabilizing factor, in this study both the Jeffrey viscoelasticity and internal heating contribute to destabilization under the chosen parameters. Consistent with literature, the salinity Rayleigh number continues to act as a stabilizing influence. Together, internal heating and viscoelasticity enhance system instabilities, initiating convection at lower thermal forcing, while the critical wave number—and hence the characteristic cell size—remains largely unchanged. This combined effect has practical significance for energy and thermal management systems, including solar collectors, geothermal reservoirs, and chemical reactors, where enhanced convection is beneficial, but flow stability must be carefully controlled.

The findings of this study are relevant for engineering systems where heat and mass transfer in nanofluids within porous structures is critical. Potential applications include enhanced oil recovery, geothermal energy extraction, solar thermal collectors, microelectronic cooling, and biomedical devices. The results may guide the design of more stable and efficient thermal systems by identifying conditions that suppress or trigger convection.

Results and Discussion

The thermal instability of binary Jeffrey nanofluid layer in porous medium is conducted by investigating the stationary thermal Rayleigh number, given by Eq. (35) and examining the effects of relevant non-dimensional parameters. The numerical computation of thermal Rayleigh numbers is performed using MATHEMATICA software (version-12), where one non-dimensional parameter is varied while keeping others constant. The parameter values are considered within certain limits. Graphical representations of the calculated results are shown in Figs. 2–8 with a specific focus on a top-heavy distribution of nanoparticles. The current analysis focuses on stationary convection to establish fundamental stability characteristics. The methodology can be adapted to investigate oscillatory and transient modes, offering insights into time-dependent convection, wave propagation, and the evolution of instabilities under varying thermal and solutal conditions.

The impact of Rayleigh number due to salinity, R_s on stationary thermal Rayleigh number R_a^s, in relation to the wave number a in the stationary mode, is depicted in Fig. 2. It is observed from the curves that a rise in the solutal Rayleigh number leads to a notable effect, resulting in an escalation of the thermal Rayleigh number. Therefore, R_s stabilizes

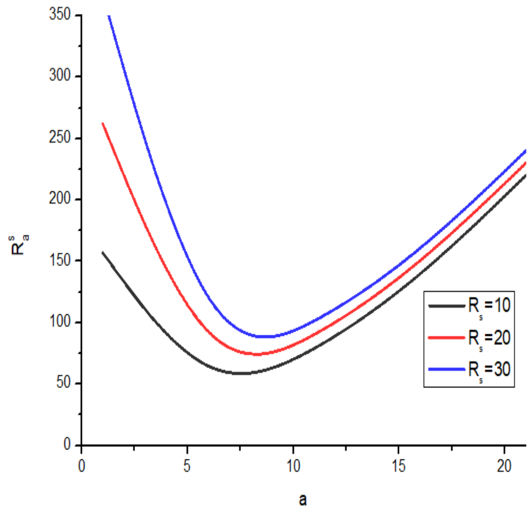

Fig. 2. Comparison ofstationary thermal Rayleigh number R_a^s against wave number a for multiple values of Rayleigh number due to salinity R_s

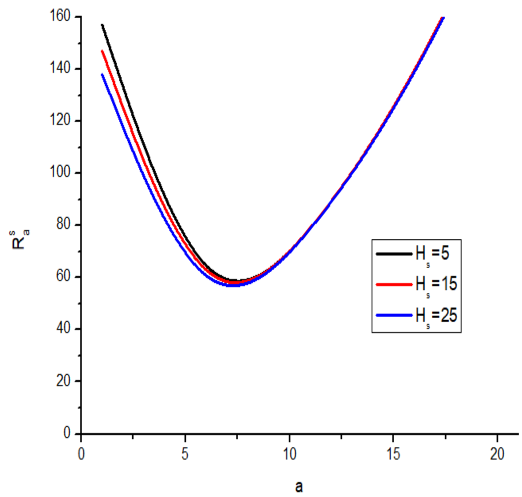

Fig. 3. Comparison ofstationary thermal Rayleigh number R_a^s against wave number a for multiple values of internal heat source H_s

the system. A large solutal Rayleigh number leads to convective instability, where buoyancy forces dominate over diffusive forces. Conversely, a small solutal Rayleigh number enhances the significance of diffusive forces, resulting in a more stable system. Physically, as salinity-induced buoyancy grows, the system resists purely thermal disturbances more effectively, thereby raising the threshold of thermal instability.

Figure 3 depicts the correlation between the internal heating parameter H_s and the thermal Rayleigh number R_a^s in the study. The results indicate that a decrease in the internal heating leads to an increase in R_a^s. As a result, the convective cell size increases, exerting a destabilizing influence on the Jeffrey nanofluid. Furthermore, the internal heat source causes a decrease in the critical wave number, thereby enhancing the convective heat transfer within the system. In physical terms, greater internal heating injects extra energy into the fluid layer, which reduces the critical condition for instability and promotes more vigorous convection in the Jeffrey nanofluid.

A visualization of the relationship between the stationary thermal Rayleigh number, R_a^s and the Jeffrey fluid parameter, λ is presented in Fig. 4. As the Jeffrey parameter increases, it is noted that the stability range for the stationary mode decreases, resulting in a decline in R_a^s. However, despite this increase, the critical wave number remains unchanged. Thus, stronger Jeffrey-type elasticity promotes earlier onset of convection by reducing the required thermal driving, even though it does not change the characteristic size of convective cells.

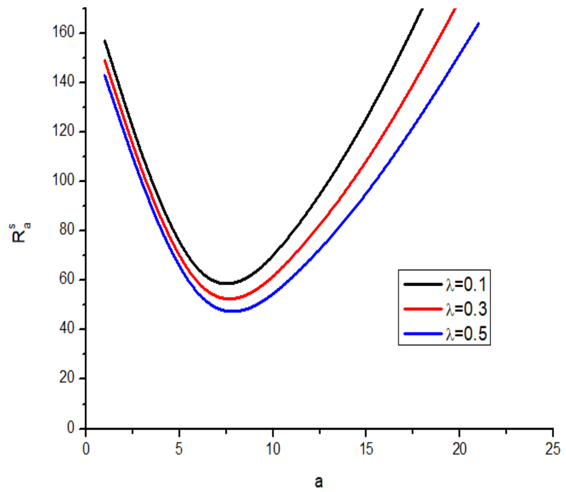

Fig. 4. Comparison ofstationary thermal Rayleigh numberR_a^s against wave number a for multiple values of Jeffrey parameter λ

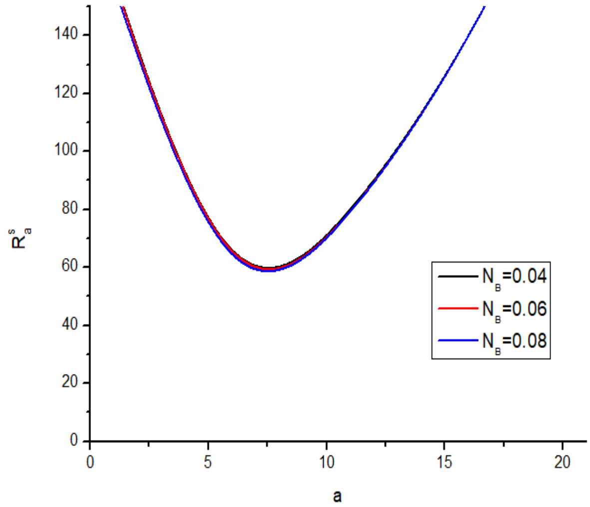

Fig. 5. Comparison ofstationary thermal Rayleigh numberR_a^s against wave number a for multiple values of modified particle density increment N_B

Figure 5 and 6 present the relationship between the modified particle density increment N_B and the concentration Rayleigh number R_n, respectively, with R_a^s. It is observed from Fig. 5 that when the modified particle density experiences a slight decrease, the thermal Rayleigh number increases due to the low value of the term NB^{-1} in the energy equation. This decrease leads to the expansion of convectional cells, thereby destabilizing the system. Conversely, Fig. 6 illustrates that as the concentration Rayleigh number rises, there is a corresponding increase in R_a^s, thus advancing the onset of stationary convection. While changes in the concentration Rayleigh number affect the critical wave number, the increment in modified particle density does not have any influence on it. Physically, this means that a reduction in modified particle density weakens the stabilizing role of nanoparticles, allowing convection to occur more easily with larger cells. In contrast, an increase in the concentration Rayleigh number enhances solutal buoyancy, which accelerates the onset of convection and also alters the size of convection cells.

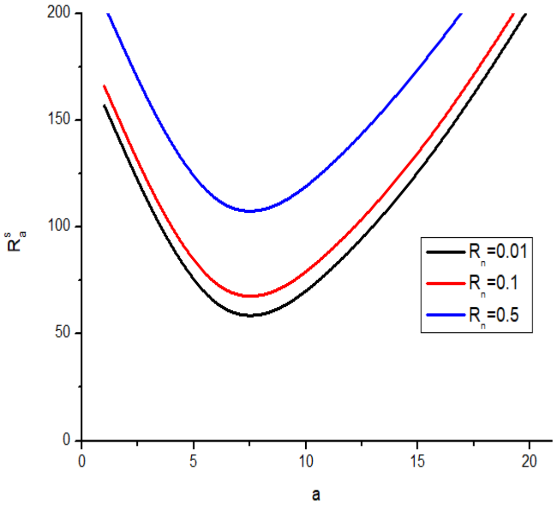

Fig. 6. Comparison of stationary thermal Rayleigh number R_a^s against wave number a for multiple values of concentration Rayleigh number R_n

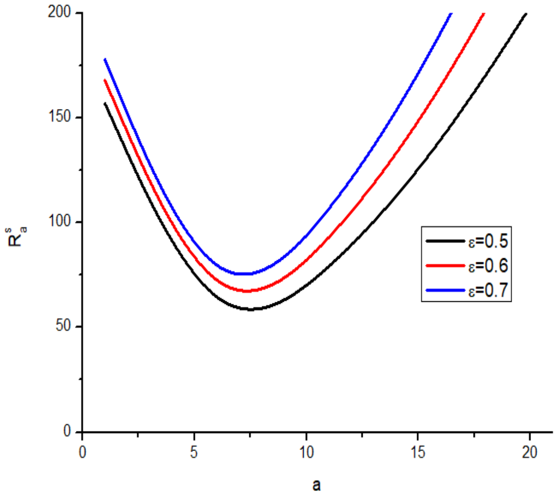

Fig. 7. Comparison of stationary thermal Rayleigh number R_a^s against wave number a for multiple values of porosity ε

In Fig. 7, the impact of medium porosity, ε on the system stability framework is depicted. As the medium porosity increases, the stationary thermal Rayleigh number R_a^s also increases, expanding the region of stability under stationary modes. Consequently, the size of convection cells decreases. Porosity represents the fraction of open space available for fluid flow within the medium. As porosity increases, the medium behaves

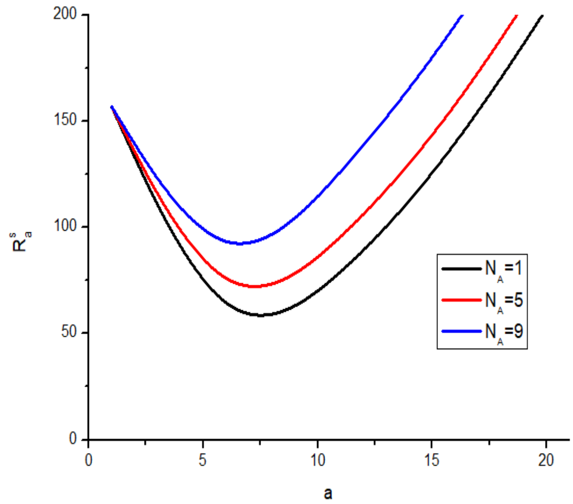

Fig. 8. Comparison of stationary thermal Rayleigh number R_a^s against wave number a for multiple values of modifieddiffusivity ratio N_A

more like a free-fluid layer with reduced resistance from the solid matrix. This facilitates fluid motion, but the enhanced heat transfer stabilizes the system, thereby raising the critical Rayleigh number. Consequently, convection is delayed to higher thermal forcing, and when it sets in, smaller convection cells are formed, allowing more efficient heat transport in the porous environment.

Figure 8 illustrates the impact of modified diffusivity ratio, N_A on R_a^s. An elevation in the modified diffusivity ratio leads to a rise in thermal Rayleigh number, which in turn amplifies the stability region and enlarges the convection cells. Consequently, the system is stabilized by modified diffusivity ratio. Nevertheless, the critical wave number remains unaltered. This implies that the system demands stronger thermal forcing to initiate convection. Although the convection cells grow in size, the fundamental spacing between them, represented by the critical wave number, does not change. In other words, stability is enhanced without altering the basic pattern of convection onset.

The observed trends in our study generally align with prior research, while showing some notable deviations. Previous investigations on viscoelastic nanofluid convection [14,23,42–45] indicate that results depend strongly on the chosen model and parameters. For example, the Jeffrey model in earlier studies (Rana [44]) typically promotes convection,porosity tends to destabilize the system, and the nanofluid parameter modified diffusivity ratio often has negligible influence. In contrast, in our study, the Jeffrey model consistently shows a destabilizing effect, porosity acts oppositely by stabilizing, and modified diffusivity ratio surprisingly produces a pronounced stabilizing effect. The Rayleigh number due to salinity, meanwhile, promotes stability, in agreement with Umavathi et al. [45]. Regarding internal heating, prior studies, including Khalid et al. [42], indicate that internal heat sources generally destabilize the system. Our results corroborate this observation, confirming that internal heating has a destabilizing influence in our configuration as well. These findings highlight the sensitivity of system stability to parameter interactions and emphasize the importance of considering mixed parameter effects when analyzing convection in viscoelastic nanofluids.

Conclusions

This paper investigates the influence of viscoelastic behavior and internal heating on double-diffusive convection in a Jeffrey nanofluid saturated porous medium. By applying linear stability theory and a one-term Galerkin approach, an analytical expression for the stationary thermal Rayleigh number was derived. Key findings reveal that higher concentration and solutal Rayleigh numbers expand the convection domain, internal heating strengthens heat transfer, while increased porosity and diffusivity ratio improve system stability. In contrast, reduced particle density and higher salinity Rayleigh numbers trigger destabilization. The Jeffrey parameter reduces stability without altering the critical wave number, underlining the distinct role of viscoelasticity.

Overall, the results provide new insights into the thermo-diffusion behavior of Jeffrey nanofluids, with potential applications in thermal energy storage, enhanced oil recovery, and polymeric material design. The analytical framework can guide the design of advanced nanofluid systems for engineering applications. Future research may extend this work to nonlinear regimes, oscillatory instabilities, fractional-order models, and AI-assisted prediction techniques, alongside experimental validation for practical systems.

CRediTauthorshipcontributionstatement

Virender Sharma: writing – review & editing, writing – original draft, data curation; **Jyoti Devi**: writing – review & editing, writing – original draft, Investigation; **Rajneesh Kumar:** conceptualization, supervision; **Veena Sharma**: conceptualization, supervision.

Conflict of interest

The authors declare that they have no conflict of interest.

References

1. Stern ME. The 'salt fountain' and thermohaline convection. *Tellus.* 1960;12(2): 172–175.
2. Huppert HE, Turner JS. Double-diffusive convection. *Journal of Fluid Mechanics.* 1981;106: 290–329.
3. Dougall J. Double diffusive convection caused by coupled molecular diffusion. *Journal of Fluid Mechanics.* 1983;126: 379–397.
4. Kafoussias NG, Williams EW. The effect of temperature-dependent viscosity on free-forced convective laminar boundary layer flow past a vertical isothermal flat plate. *Acta Mechanica.* 1995;110: 123–137.
5. Kuznetsov G, Sheremet M. A numerical simulation of double-diffusive conjugate natural convection in an enclosure. *International Journal of Thermal Sciences and Physical Engineering.* 2011;50(10): 1878–1886.
6. Lotfy K, El-Bary AA, Hassan W, Ahmed MH. Hall current influence of microtemperature magneto-elastic semiconductor material. *Superlattices and Microstructures.* 2020;139: 106428.
7. Lotfy K, Elidy ES, Tantawi RS. Photothermal excitation process during hyperbolic two-temperature theory for magneto-thermo-elastic semiconducting medium. *Silicon.* 2021;13(7): 2275–2288.
8. Lotfy K, El-Bary AA. Magneto-Photo-Thermo-Microstretch Semiconductor Elastic Medium Due to Photothermal Transport Process. *Silicon.* 2022;14(9): 4809–4821.
9. Ismail GM, Gepreel KA, Lotfy K, Mahdy AMS, El-Bary A. Influence of variable thermal conductivity on thermal-plasma-elastic waves of excited microelongatedsemiconductor. *Alexandria Engineering Journal.* 2022;61(12): 12271–12282.
10. Choi SU. Enhancing thermal conductivity of fluids with nanoparticles. In: *Developments and Applications of Non-Newtonian Flows*. 1995. p.231–247.
11. Maxwell JC. On the dynamical theory of gases. *Journal of Phil. Trans. R. Soc. London*. 1866;157: 2678.
12. Xuan Y, Li Q. Heat transfer enhancement of nanofluids. *International Journal of Heat and Mass Transfer.* 2000;21(1): 58–64.
13. Buongiorno J. Convective transport in nanofluids. *Journal of Heat Transfer.* 2006;128(3): 240–250.
14. Umavathi JC, Sasso M. Double diffusive convection in a porous medium layer saturated with an Oldroyd nanofluid. *AIP Conference Proceedings.* 2017;1798: 020166.
15. Yadav D, Kumar Awasthi M, Al-Siyabi M, Al-Nadhairi S, Al-Rahbi A, Al-Subhi M, et al. Double diffusive convective motion in a reactive porous medium layer saturated by a non-Newtonian Kuvshiniski fluid. *Physics of Fluids.* 2022;34(2): 024104.
16. Shoaib M, Rafia T, Raja MAZ, Khan WA, Waqas M. Further analysis of double-diffusive flow of nanofluid through a porous medium situated on an inclined plane: AI-based Levenberg–Marquardt scheme with backpropagated neural network. *Journal of the Brazilian Society of Mechanical Sciences and Engineering.* 2022;44: 227.
17. Sparrow EM, Tsou FK, Kurtz Jr EF. Stability of Laminar Free-Convection Flow on a Vertical Plate. *The Physics of Fluids.* 1965;8(8): 1559–1561.
18. Watson PM. Classical cellular convection with a spatial heat source. *Journal of Fluid Mechanics.* 1968;32(2): 399–411.
19. Israel-Cookey C, Nwaigwe C. Unsteady MHD flow of a radiating fluid over a moving heated porous plate with time-dependent suction. *American Journal of Scientific and Industrial Research.* 2010;1(1): 88–95.
20. Yadav D, Bhargava R, Agrawal GS. Boundary and internal heat source effects on the onset of Darcy–Brinkman convection in a porous layer saturated by nanofluid. *International Journal of Thermal Sciences.* 2012;60: 244–254.
21. Sharma S, Sharma K. Influence of heat sources and relaxation time on temperature distribution in tissues. *International Journal of Applied Mechanics and Engineering.* 2014;19(2): 427–433.

22. Altawallbeh AA. Cross diffusion effect on linear and nonlinear double diffusive convection in a viscoelastic fluid saturated porous layer with internal heat source. *Fluids.* 2021;6(5): 182.
23. Bouazizi L, Turki S. Combined effects of viscous dissipation and Brownian motion on temperature distribution and heat transfer of Al_2O_3/water nanofluid flow through a porous medium. *Materials Physics and Mechanics.* 2021;47(6): 921–936.
24. Sharma S, Khator S. Micro-grid planning with aggregator's role in the renewable inclusive prosumer market. *Journal of Power and Energy Engineering.* 2022;10(4): 47–62.
25. Sharma S, Khator S. Power generation planning with reserve dispatch and weather uncertainties including penetration of renewable sources. *International Journal of Smart Grid and Clean Energy.* 2021;10(4): 292–303.
26. Ali SA, Rudziva M, Sibanda P, Noreldin OAI, Goqo SP, Mthethwa HS. A numerical study of double-diffusive convection in the anisotropic porous layer under rotational modulation with internal heat generation. *International Communications in Heat and Mass Transfer.* 2022;137: 106266.
27. Syzrantsev VV, Arymbaeva AT, Zavjalov AP, Zobov KV. The nanofluids' viscosity prediction through particle-media interaction layer. *Materials Physics and Mechanics.* 2022;48(3): 386–396.
28. Abo-Dahab SM, Mohamed RA, Abd-Alla AM, Soliman MS. Double diffusive peristaltic MHD Siskonanofluid flow through a porous medium in presence of non-linear thermal radiation, heat generation/absorption, and Joule heating. *Scientific Reports.* 2023;13: 1432.
29. Paandurangan B, Parthasarathy SE, Tripathi D, Bég OA. The impact of double-diffusive convection on electroosmotic peristaltic transport of magnetized Casson nanofluid in a porous asymmetric channel. *Zeitschrift für AngewandteMathematik und Mechanik.* 2024;104(9): e202300771.
30. Alanazi K, Abouelregal AE. Thermoelastic behavior of infinite porous media with voids subjected to instantaneous heat Sources: A Spatio-Temporal nonlocal and fractional heat transfer approach. *Ain Shams Engineering Journal.* 2025;16(7): 103377.
31. Xu W, Liu H, Chen L, Zhou Y. Ultrafast diffusion modeling via the Riemann–Liouville nonlocal structural derivative and its application in porous media. *Fractal and Fractional.* 2024;8(2): 110.
32. Zhang X, Zeng S. Time-space fractional porous medium equations with nonlocal nonlinear terms. *Evolution Equations and Control Theory.* 2025;14(6): 1678–1695.
33. Junaid MS, Aslam MN, Khan MA, Saleem S, Riaz MB. Thermal analysis of a viscoelastic Maxwell hybrid nanofluid with graphene and polythiophene nanoparticles: Insights from an artificial neural network model. *Alexandria Engineering Journal.* 2024;94: 193–211.
34. Bocanegra JA, Marchitto A, Misale M. Nanofluids in solar collectors: a comprehensive review focused on its sedimentation. *Clean Technologies and Environmental Policy.* 2025;27(4): 1753–1784.
35. Raza M, Faiz M, Hassan WU, Abbas M, Raza J, Kumail Z, Nawaz T, Shabir S, Jan A, Li FC. AI-powered optimization and numerical techniques for nanofluid heat transfer systems-a review. *Multiscale and Multidisciplinary Modeling, Experiments and Design.* 2024;8(7): 316.
36. Nield DA, Kuznetsov AV. The onset of convection in a horizontal nanofluid layer of finite depth. *European Journal of Mechanics-B/Fluids.* 2010;29(3): 217–223.
37. Nield DA, Kuznetsov AV. The onset of double-diffusive convection in a nanofluid layer. *International Journal of Heat and Fluid Flow.* 2011;32(4): 771–776.
38. Kuznetsov AV, Nield D. The onset of double-diffusive nanofluid convection in a layer of a saturated porous medium. *Transport in Porous Media.* 2010;85: 941–951.
39. Gupta U, Kaur J. Nanofluids rheology for viscoelastic Oldroyd-B fluid: a revised model. *Journal of Physics: Conference Series.* 2020;1531: 012052.
40. Sandeep N, Sulochana C. Momentum and heat transfer behaviour of Jeffrey, Maxwell and Oldroyd-B nanofluids past a stretching surface with non-uniform heat source/sink. *Ain Shams Engineering Journal.* 2018;9(4): 517–524.
41. Lapwood E. Convection of a fluid in a porous medium. *Mathematical Proceedings of the Cambridge Philosophical Society.* 1948;44(4): 508–521.
42. Khalid IK, Mokhtar NFM, Hashim I, Ibrahim ZB, Gani SSA. Effect of internal heat source on the onset of double-diffusive convection in a rotating nanofluid layer with feedback control strategy. *Advances in Mathematical Physics.* 2017;2017(1): 2789024.
43. Rana GC, Thakur RC, Kango SK. On the onset of double-diffusive convection in a layer of nanofluid under rotation saturating a porous medium. *Journal of Porous Media.* 2014;17(8): 88–95.
44. Rana GC. Effects of rotation on Jeffrey nanofluid flow saturated by a porous medium. *Journal of Applied Mathematics and Computational Mechanics.* 2021;20(3): 17–29.
45. Umavathi JC, Sheremet MA, Ojjela O, Reddy GJ. The onset of double-diffusive convection in a nanofluid saturated porous layer: Cross-diffusion effects. *European Journal of Mechanics-B/Fluids.* 2017;65: 70–87.